Oscillations of low-current electrical discharges between parallel-plane electrodes. II. Pulsed discharges in H_2

B. M. Jelenković,* K. Rózsa,† and A. V. Phelps‡
Joint Institute for Laboratory Astrophysics, University of Colorado and National Institute of Standards and Technology, Boulder, Colorado 80309-0440
(Received 29 October 1992)

Measurements are made of damped oscillations in the current and voltage induced by a voltage pulse applied to the stabilizing resistor of discharges in H_2 at pressure times electrode spacing values of 0.3 to 1 Torr cm (40–133 Pa cm) operating at voltages of 300 to 2100 V. The use of pulses ≤ 1 ms long and repetition rates of 10 Hz results in low ion bombardment of the cathode. For pulse currents of 0.01 to 5 mA (2×10^{-7}–10^{-4} A/cm^2) and an electrode separation and area of 1 cm and 50 cm^2, the frequencies and damping constants are 10–300 kHz and 2×10^3–10^5 s^{-1}, respectively. The current densities are small enough so that space-charge distortion of the electric field is small, but not negligible. At currents below those for oscillation growth, the steady-state discharge voltage decreases as expected for a constant negative differential resistance. Values of 1000 to 4000 Ω are obtained depending on pressure and cathode condition. Transient models, developed in an accompanying paper, relate the frequencies, damping constants, and onset of oscillation growth to ion transit times, electron ionization coefficients, and ion-induced electron yields. The growth of discharge current immediately after the application of the voltage pulse is also used to determine discharge parameters.

PACS number(s): 52.80.Dy, 52.80.Hc, 52.40.Hf

I. INTRODUCTION

This is the second in a series of papers, designated papers I [1], II, and III [2], in which we describe measurements of the electrical behavior of low-current electrical discharges in low-pressure hydrogen between parallel-plane electrodes and compare them with simple models. The effects of the measurement on the electrode and discharge properties are greatly reduced from those of dc experiments, such as discussed in I, by replacing the laser-induced photoelectron source by a pulsed voltage and by using a nonintrusive current monitor. The principal experimental results are measurements over a wider range of pressures of the negative differential resistance of the discharge and of the frequency and damping constant for oscillations induced by the voltage pulse. These results are found to be in good agreement with the simple model of the discharge developed in paper III of this series [2].

Pulsed electrical discharges in hydrogen have been the subject of numerous investigations because of the unique ability of these discharges to recover their insulating properties quickly [3–5]. More recently, the development of the discharge has been examined because of the interest in fast, high-current switching discharges, called pseudosparks [5]. Closely related to the present work are the measurements by Morgan [6], by Jones and Llewellyn-Jones [6], and by Graf and Schmitz [7] of current growth in H_2 discharges subject to small overvoltages and small currents. Schlumbohm [8] followed the growth of current at low pressures until the effects of space-charge distortion of the electric field was significant. For a single set of discharge conditions, he obtained very good agreement between experiment and theory. Nahemow and Wainfan [9] and Nahemow, Wainfan and Ward [10] considered the development of the cathode fall when H_2 is subjected to a large voltage pulse and to currents well above those considered here. Pulsed techniques were used for a wide range of discharge currents and pressures by Klyarfel'd, Guseva, and Pokrovskaya-Soboleva [11] to avoid cathode heating. The present paper is concerned with small overvoltages and currents that lead to small space-charge distortion of the electric field. Very recent experiments in our laboratory [12] extend the present measurements to moderate currents and to the highly nonuniform electric fields characteristic of a fully developed cathode fall. We are not concerned with the large space-charge-induced distortions of the electric field that lead to the development of streamers and arcs [13].

Measurements and analyses are reported of the current oscillations following sudden increases in current through low-current, low-pressure discharges in hydrogen. The current densities are small enough so that the calculated space-charge distortion of the electric field was small, but not negligible. The E/n values (E/n is the ratio of the electric field E to the gas density n) range from E/n for which the electrons are in equilibrium with the gas to very high E/n where nonequilibrium effects have been observed in H_2 [14]. As the pulse voltage applied to a very low-current dc discharge is increased the transient voltage and current wave forms change from an overdamped wave form to a damped oscillation, to growing oscillations, to damped oscillations, and finally to overdamped wave forms. The region of growing oscillations during the voltage pulse corresponds to the region of self-sustained oscillations observed with dc discharges in paper I and in earlier work [15,16]. The greater stability

and sensitivity of the pulse technique allowed measurements in both the lower and upper regions of damped oscillations. Our principal interest is in the measurement of damped oscillations at the lower currents and their comparison with a simple model developed in paper III. The frequencies of the damped oscillations ranged from 10 to 300 kHz and the damping time constants were 10 μs to 0.5 ms. Only very limited records were saved of data in the region of currents resulting in growing or undamped oscillations or of overdamped oscillations. The present damped oscillation experiments complement the earlier impedance measurements for hydrogen discharges by Sigmond [15] at higher pressures and a smaller electrode separation.

The experimental apparatus is described in Sec. II. Representative current and voltage wave forms are discussed in Sec. III. Measurements of quasi-steady-state voltage-current characteristics are presented in Sec. IV. The results of measurements of the transient oscillations resulting from the application of a pulse to the discharge circuit are compared with theory in Sec. V. In Sec. VI we present the results of current growth measurements in these discharges.

II. EXPERIMENT

The experiments were conducted in the discharge tube described in Fig. 1 of paper I and most of the data reported were obtained with the electrical circuit shown in Fig. 1 of this paper. The pressures were varied from 0.5 to 3 Torr for an electrode separation of 1.05 cm and an electrode area of 50 cm^2. The dc voltage used to maintain the discharge between pulses is supplied from a voltage-regulated supply V_1 through the resistors R_1 and R_S. The isolation resistor R_1 was usually 20 kΩ and the resistance R_S was varied from 10^4 to 5×10^6 Ω. The voltage pulses are supplied to R_S from the pulse generator through a large capacitance. The discharge current was measured with a wide-band ($\approx$200 MHz) operational amplifier so as to keep the anode at ground potential and make the effective monitor resistor R_m of paper I equal to zero. The operational amplifier output was recorded with a wide bandwidth (200 MHz) storage oscilloscope. Similarly, the time-varying voltage across the discharge tube was measured with a high-impedance compensated voltage divider rated at $\approx$5-MHz bandwidth and recorded by the oscilloscope. A photomultiplier was used to observe the H_α emission with a measured response time of <100 ns and recorded with the oscilloscope. The oscilloscope output was transferred to a personal computer for disk storage and analyses.

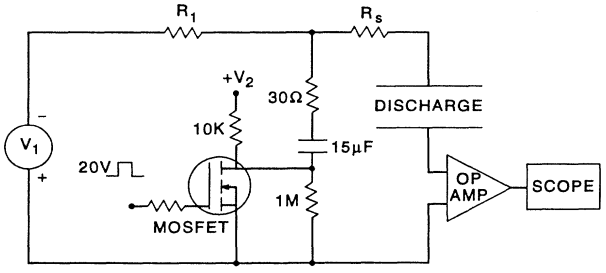

FIG. 1. Schematic of electrical circuit showing the MOSFET semiconductor device used to generate the high-voltage pulse and the operational amplifier used to monitor current.

The voltage pulses were produced by applying a 15–20 V pulse to the gate of a metal-oxide-semiconductor field-effect transistor (MOSFET) and typically lasted for 0.1 to 1 ms. The low impedance ($\approx$2 Ω) of the MOSFET drops the voltage at the low side of the coupling capacitor to essentially ground potential. The large capacitor (15 μF) couples the voltage pulse to the series resistor R_S. Oscilloscope measurements showed that the voltage developed at the junction of R_1 and R_S was a flat-topped pulse during the times that the discharge voltage was oscillating. Therefore R_S is the effective damping resistor for the pulsed experiment and R_1 can be neglected in the data analysis. With this circuit we obtain up to 1000 V pulses with a rise time of about 100 ns and a nearly constant voltage for several ms. The large voltage pulses allow operation of the discharge at pulsed currents up to 100 mA for $R_S\approx5$ kΩ.

The use of a pulsed voltage rather than a dc voltage to develop the high currents minimizes the bombardment of the cathode and the resultant changes in the cathode condition. For a 1-mA/cm^2 (50-mA total current) pulse lasting for 100 μs, less than 10^{12} ions/cm^2 strike the cathode per pulse. This means bombardment by less than the equivalent of 1% of a monolayer. The fast atom flux may be several times this amount [17]. For a pulse repetition frequency of 10 Hz, the ion flux bombarding the cathode between pulses is usually comparable with that during pulses. Typically, the present experiments use 16 transients to obtain a good signal-to-noise ratio, although useful data can be obtained from one transient at the higher currents. Because of the reduced rate of drift of the cathode conditions, one can measure small changes in frequency or in the "steady-state" discharge voltage with considerably more accuracy than with the dc discharge of paper I.

Gas pressures are measured with a diaphragm-type manometer with a stated accuracy of ±0.01 Torr, where 1 Torr$=$133 Pa. The gas samples were taken from high-pressure cylinders with a stated purity of 0.9999. The rate of rise of pressure after overnight evacuation and mild baking is $\approx5\times10^{-4}$ Torr/h. Unless noted otherwise, the discharges are uniform in the radial direction as reported in paper I and as observed visually from the side of the discharge tube.

Considerable difficulty was encountered in obtaining reproducible low-current dc discharge operating voltages V_B. Especially at 0.5 Torr, the discharge voltage at currents below about 1 μA was found to increase considerably, e.g., almost double, as the discharge was operated. As observed previously [6,18], the change in discharge voltage correlates with changes in the effective photoelectric threshold [19], i.e., the photon energy at which the photoelectric current reached 10% of its maximum value. Using an Xe arc lamp and monochromator as a source, the photoelectric threshold increased from 3.4 to 4.2 eV as the discharge operating voltage increased from 365 to 650 V at $p=0.5$ Torr. An aging procedure in

which the discharge was operated for ≈ 10 min at a current of 0.5 mA and a pressure of 1 Torr of H_2 was adopted that resulted in voltages that were reproducible to ± 5 V and drifted < 10 V/h. On the basis of the data from paper I, this aging current gives a radially uniform discharge.

III. VOLTAGE-CURRENT WAVE FORMS

Representative voltage, current, and optical emission transients in response to a pulse of voltage applied to R_S are shown by the curves in Fig. 2. The voltage and current wave forms from the model of paper III are shown by the points. The applied voltage pulse (not shown) has a 100-ns rise time to a magnitude of 27 V and for $R_S = 100$ kΩ produced a 1-V decrease in discharge voltage and a steady-state current of 260 μA. Since the magnitude of the voltage pulse used to obtain a given set of discharge conditions depends on the value of R_S, we characterize individual measurements by the steady-state discharge current I_{SS} rather than the amplitude of voltage pulse. The initial rise in the voltage across the discharge is determined by the time constant of the circuit with no discharge, i.e., $R_S C = 25$ μs for Fig. 2, where C is the total circuit capacitance and is primarily due to cable capacitance. Note that initiating electrons are provided by weak dc discharge operating at ≈ 10 μA in Fig. 2. A small initial current step (not observable in Fig. 2) is caused by the displacement current flowing between the discharge electrodes as a result of the approximately linear increase in discharge voltage for the first few microseconds. The initial increase of the electron and ion currents through the discharge will be shown in Sec. VI to follow the predictions of the model of paper III. Eventually the discharge current becomes large enough for the voltage drop across R_S and the charge loss from C to cause a decrease in discharge voltage. The current and voltage then follow a damped oscillation until they reach a steady state. Note that the small changes in the voltage wave form, e.g., $< 15\%$ of the average discharge voltage, are much more sinusoidal than are the large fractional changes in the current wave form. The changes in voltage and current at the end of the applied pulse at 550 μs in Fig. 2 are slow because of the high impedance and slow recovery of the MOSFET modulator.

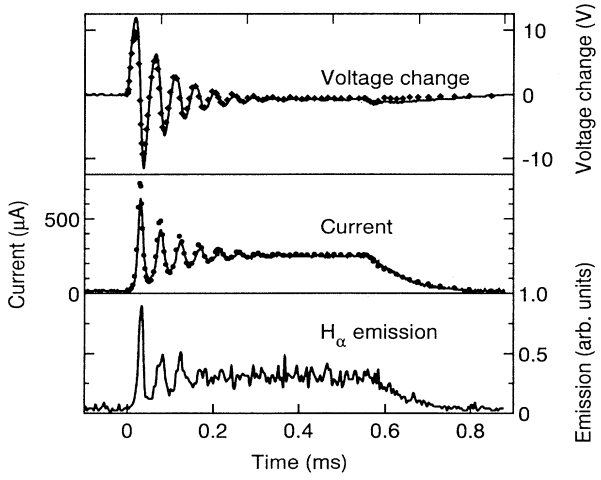

FIG. 2. Representative voltage, current, and optical emission wave forms in response to a rectangular pulse of voltage (not shown) applied to the series resistor. Note the ≈ 0.8-V decrease in voltage for an increase in steady-state current from 20 to 260 μA. The solid curves are experiment and the points are calculated using the model of paper III. $pd = 0.525$ Torr cm, $R_S = 10^5$ Ω, and $V_B = 707$ V.

When the amplitude of the voltage pulse is raised to sufficiently large values the amplitude of successive current maxima increases with time during the pulse. This transition from damped oscillations to growing or undamped oscillations corresponds to the transition from damped oscillations to self-sustained oscillations in paper I. Some differences may occur because the current peaks are too large to be described by the small-signal model developed in paper III. In many cases the "growing" oscillations reached their final form too quickly for the growth of successive cycles to be observed.

The fits of the model to the experimental current and voltage wave forms shown by the points of Fig. 2 were obtained by solving Eq. (10) and (11) of paper III. The only adjustable constants in the calculation of these wave forms are the amplitude of the voltage pulse and the decay constant of the driving voltage wave form, which was not measured. The effective ion transit-time, the electron-impact ionization coefficient, and ion-induced secondary emission yield used in the model are obtained from fit of the model to angular frequency data and to the discharge maintenance voltage data extrapolated to zero current. This procedure is discussed in Sec. IV and in the Appendix of paper III.

Figure 2 also shows the time dependence of light emission obtained using a photomultiplier and interference filter peaked at H_α. The time dependence of the H_α emission follows very closely the time dependence of the discharge current. As assumed in the model of paper III, this behavior results from the short transit time of the electrons and hydrogen ions compared to the oscillation period.

IV. VOLTAGE-CURRENT CHARACTERISTICS AND NEGATIVE RESISTANCE

In this section we are concerned with the change in quasi-steady-state voltage from that used to maintain the discharge at low currents, e.g., the change of -0.8 V between $t < 0$ and $t \approx 350$–550 μs for a current change of 260 μA (5.2 μA/cm^2) in Fig. 2. Figure 3 shows the measured quasi-steady-state discharge voltages for pressures of 0.5 and 1 Torr as a function of quasi-steady-state discharge current I_{SS}. These plots differ from the voltage-current plots of Fig. 3 of paper I in that the pulse technique yields much more accurate values for the negative voltage changes than does the dc experiment with its continually changing cathode conditions. Note that we have plotted the measured voltages as a function of current density because we expect the volt-ampere plot and the lower limit for the undamped oscillation region to scale with current density as the electrode area is

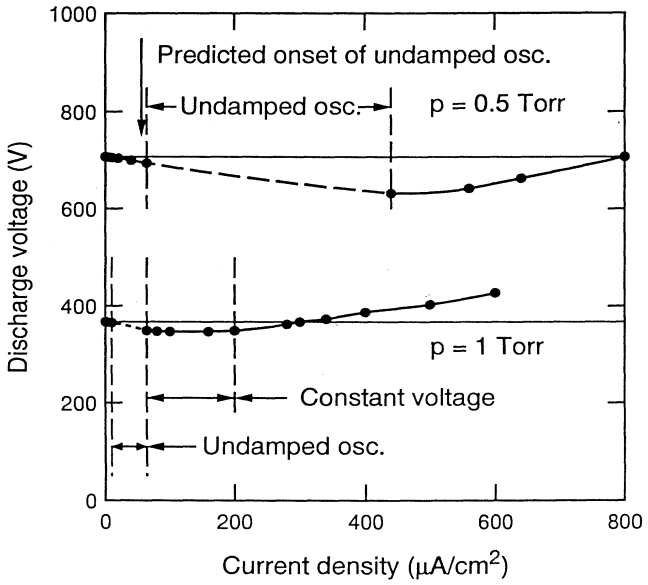

FIG. 3. Discharge voltage vs quasi-steady-state current density for $p=0.5$ and 1 Torr and $R_S=20$ kΩ. The curves are drawn through the points as a visual aid. Data are not available for the dashed sections because of undamped or self-sustained oscillations throughout the current pulse. The arrow shows the predicted onset of undamped oscillations using the small-signal model of paper III. Note the presence of a region for which the voltage is independent of current for $p=1$ Torr.

changed at fixed p, R_S, and C. See Secs. III and IV of paper III. We note that the low-current limit of the discharge voltage is equal to the minimum breakdown voltage at low initiating currents and we will refer to this limit as the breakdown voltage V_B. The values of the breakdown voltage increase considerably as the cathode is aged by operating the discharge, especially when operated at >100 μA/cm^2. We have adopted the breakdown voltage as the measure of the cathode condition.

Models of the cathode fall applicable at current densities typical of the upper limit for undamped oscillations also predict scaling of the discharge voltage with current density as the electrode area is changed [20,21]. The hysteresis effects often seen in voltage versus current data [1,20,21] are not observed. For $pd=0.525$ Torr cm, damped oscillations are observed over the current range from 4 to 64 μA/cm^2 (0.2 to 3.2 mA). For $64<I_{SS}<440$ μA/cm^2 we observe either growing oscillations or undamped oscillations during the applied pulse. These oscillations have been labeled "undamped" in Fig. 3 and correspond to the self-sustained oscillations of Sec. IV of paper I. At I_{SS} below 4 μA/cm^2 and above 440 μA/cm^2 the current and voltage transients are overdamped. The dashed lines in the region of oscillations for both pressures are estimates of voltage change expected if the oscillations were suppressed as discussed in Sec. III C of paper III.

The data of Fig. 3 show that for $p=1$ Torr ($pd=1.05$ Torr cm) the regions of damped and undamped oscillations are shifted to lower currents compared to those for $pd=0.5$ Torr cm in agreement with the dc results of paper I. In this case, damped oscillations are also observed at average current densities of 80 and 100 μA/cm^2, i.e., they occur in the region of constant voltage versus current for which constricted discharges are usually observed. Apparently this region of constrictions was not observed in paper I because the use of widely spaced R_S values.

We see from Fig. 3 that the voltage change from the breakdown voltage is negative for currents below about 700 μA/cm^2 at 0.5 Torr and 300 μA/cm^2 at 1 Torr. In particular, the voltage change shown in Fig. 3 for the discharge operating with $pd=0.525$ Torr cm extrapolates directly with the current for currents up to 440 μA/cm^2, i.e., the discharge appears to have a constant negative differential resistance. The constant negative differential resistance behavior is also found for $p=0.35$ and 1 Torr, as shown by the data of Fig. 4.

The points of Fig. 4 show measured voltage changes ΔV versus steady-state current for low currents and H_2 pressures from 0.35 to 1 Torr and for an electrode separation of 1.05 cm. Various series resistances were used as appropriate to the available voltage-pulse amplitudes and desired currents, e.g., R_S was varied from 1 MΩ for the lowest currents shown to 20 kΩ for the highest currents. The solid line through the data corresponds to differential resistance R_D of -3.4 kΩ or a normalized negative differential discharge resistivity $R_N=R_D A/d^2$ of -170 kΩ. Here A is the electrode area and d is the electrode separation. While the values of R_D shown in Fig. 4 are very consistent, measurements with unpro-

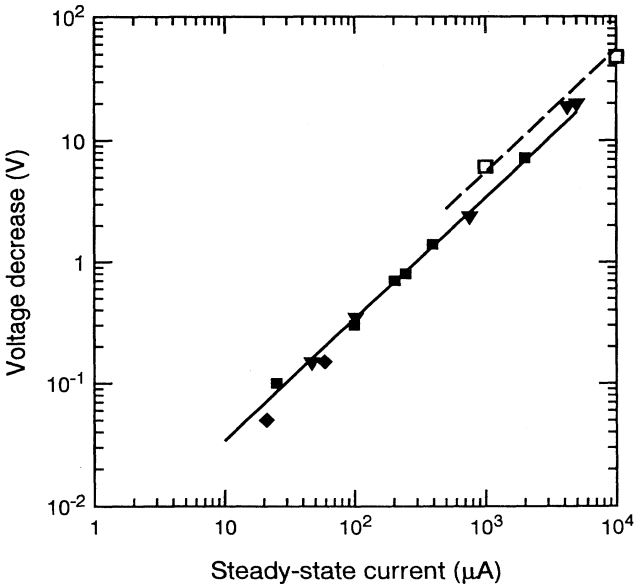

FIG. 4. Voltage decrease vs steady-state current for various pressures at currents below and above the region of growing oscillations. The solid straight line corresponds to a constant discharge differential resistance of -3.4 kΩ. The symbols and gas pressure are ♦, 0.35 Torr; ●, 0.5 Torr; ■, 1 Torr. The open squares are the results of numerical calculations using a nonequilibrium electron and ion model as discussed in paper III.

cessed cathodes are very badly scattered. Previous measurements [15,22,23] of voltage-current characteristics for similar discharges in H_2 yield values for the normalized negative resistivity R_N range from 100 kΩ to 3 MΩ. The available data will be compared with theory for hydrogen in Sec. IV A of paper III. Also, the open squares of Fig. 4 show approximate agreement between the predictions of the numerical model of Sec. IV B of paper III for $pd=0.5$ Torr cm and experiment.

We next consider an implication of the absence of a pressure dependence for the values of R_D derived from the sets of data of Fig. 4. The conventional [2,20,21] scaling laws for discharges for which multistep ionization, radiative loss, etc. are unimportant are that the observable quantities, e.g., discharge voltages V_B, V, and ΔV, should scale with I/p^2 and pd or more correctly, j/n^2 and nd. See paper III for further discussion of scaling. The absence of a pressure dependence for the data of Fig. 4 for $d=1.05$ cm suggests that ΔV is proportional to $I/p^2(pd)^2=Id^2$. An attempt to test the scaling with d was unsuccessful because of difficulties in obtaining reproducible cathode conditions.

V. VOLTAGE-PULSE-INDUCED DISCHARGE OSCILLATIONS

In this section we are concerned with the angular frequencies ω and damping constants κ obtained from analyses of voltage wave forms such as that of Fig. 2. Since the theory for the frequency and damping constant is a small signal theory, the fitting of the damped sinusoid is limited to times when the voltage oscillations have decayed to only a few percent of the discharge voltage and the current oscillations to less than 20% of the discharge current. The functional forms used to fit the current i and voltage v data are

$$i(t)=D\exp(-\kappa t)\sin(\omega t+\phi_1) \tag{1}$$

and

$$v(t)=G\exp(-\kappa t)\sin(\omega t+\phi_2)\ , \tag{2}$$

where ω is the angular frequency, κ is the damping constant, and ϕ_1 and ϕ_2 are the phase shifts. Measured angular frequencies and damping constants obtained from fits to experimental current and voltage wave forms are shown in Figs. 5 and 6 as a function of the pulsed discharged current. No attempt has been made to analyze the phase-shift data. The series resistance R_S used varied from 20 kΩ for the four highest currents, through 10 kΩ for six intermediate currents, to 1 MΩ for three lower currents so as to obtain the desired steady-state currents with the available voltage pulses. These data were obtained using an "aged" cathode.

A number of authors have developed models of the response of parallel-plate discharges at low current to ac voltages. In general, these models are the frequency representations of temporal models used in the present experiments. The relevant aspects of earlier work have been reviewed and the temporal models developed in paper III. The present model assumes that (i) space-charge distortion of the electric field is small but not negligible,

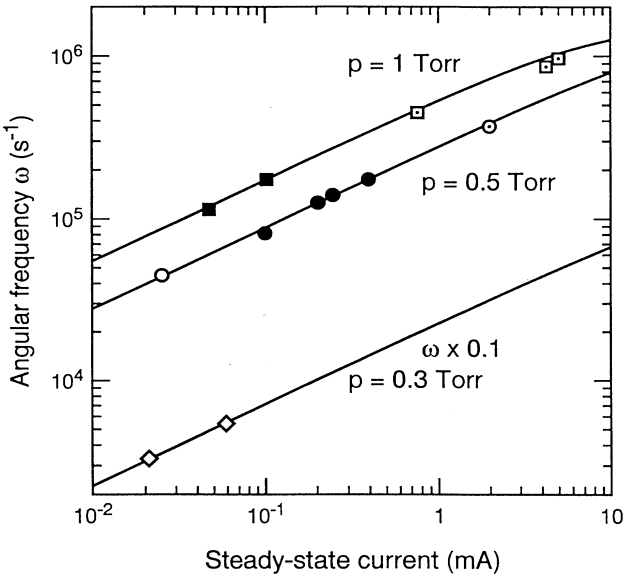

FIG. 5. Angular frequency vs current for pulsed discharges in H_2 for $d=1.05$ cm and $A=50$ cm^2. At each pressure, the line results from fitting Eqs. (3) and (4) to the experimental points by adjustment of the parameter LI_{SS}. The squares, circles, and diamonds are for pressures of 1, 0.5, and 0.3 Torr, respectively. The open points with central dots, the solid points, and the open points are for series resistances R_S of 20 kΩ, 100 kΩ, and 1 MΩ, respectively.

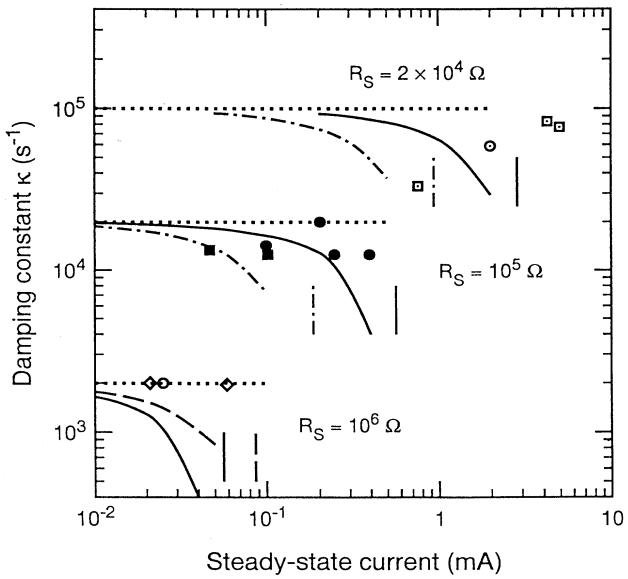

FIG. 6. Damping constant vs current for pulsed discharges in H_2 for $d=1.05$ cm. The upper set of lines and data is for $R_S=2\times10^4$ Ω, the middle set for 10^5 Ω, and the lower data for 10^6 Ω. The square points and dot-dashed lines are experiment and theory for $p=1$ Torr. Similarly, the circular points and solid lines are for $p=0.5$ Torr, and the diamond points and dashed lines are for $p=0.3$ Torr. The vertical lines are the predicted currents for the transitions from damped to growing oscillations. The dotted lines are values of $(2R_SC)^{-1}$ and are the low-current limits of κ for the various R_S values.

(ii) times for significant changes in the electric field and current are long compared to the ion transit time, (iii) electron-impact ionization is given by the local-field-equilibrium model, and (iv) secondary electrons are produced at the cathode only by ions and fast neutrals with a yield that varies with the discharge voltage and with the discharge current as the result of space-charge-induced changes in the electric field at the cathode. Although the neglect of photon-induced electron emission at the cathode has been shown to be in error for hydrogen at $E/n < 1000$ Td [6,7], we will retain the formalism of ion feedback and discuss deviations from this model in paper III.

The results of the model are usually expressed in terms of equivalent lumped-circuit elements, such as shown in Fig. 7 and discussed in more detail in paper III. For appropriate values of the circuit parameters, the application of a voltage pulse results in damped oscillations of the current through the discharge inductance L and differential resistance R_D and voltage across the capacitance C, such as shown in Fig. 2. Figures 5, 6, and 8 show comparisons of the theory and experiment for the angular frequencies, damping constants, and equivalent discharge inductances. When $\omega^2 \gg \kappa^2$, the model gives the angular frequency ω as approximately

$$\omega^2 = \frac{1}{LC}\left[1 - \frac{(-R_D)}{R_S}\right], \tag{3}$$

where the equivalent discharge inductance L and resistance R_D are discussed in III and are defined by

$$L = \frac{T}{I_{SS}\partial g/\partial V} \tag{4}$$

and

$$R_D = \frac{k_I}{\gamma_{SS}\partial g/\partial V}\,. \tag{5}$$

Here $\partial g/\partial V$ is the change in round-trip electron number gain with voltage, $k_I = \partial\gamma/\partial I_{SS}$ is the change in electron emission per unit current caused by space-charge-induced electric fields, γ_{SS} is the steady-state value of the ion-induced secondary emission coefficient, and T is the effective ion transit time. A detailed discussion of the differential resistance R_D is given in Sec. IV of paper III. According to Eqs. (3)–(5) the angular frequencies vary approximately as the square root of the discharge current as found previously [15] and as shown by the curves for each pressure in Fig. 5. The deviations of values of ω given by Eq. (3) from those calculated using the complete Eq. (20) of paper III are small for the circuit parameters and currents of the experimental data in Fig. 5.

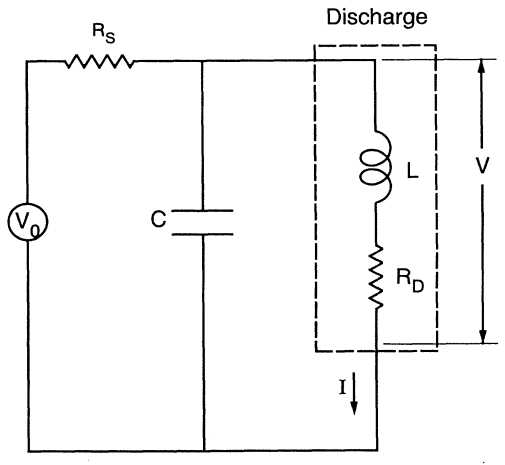

FIG. 7. Schematic of equivalent circuit form of small-signal model of pulsed discharges in H_2.

The experimental points in Fig. 5 are obtained by fitting Eqs. (1) and (2) to data such as that of Fig. 2. The series resistances R_S used were smaller for higher currents I_{SS} and are indicated by the choice of symbol. For each pressure a value of $LI_{SS} = T/(\partial g/\partial V)$ is chosen to fit Eqs. (3) and (4) to the experimental angular frequencies using the measured differential resistance R_D. The resultant theoretical curves in Fig. 5 agree well with the experimental points over the full range of currents examined.

The damping constant κ given by the model of paper III is approximately

$$\kappa = \frac{1}{2R_SC} - \frac{(-R_D)I_{SS}}{2(LI_{SS})}\,. \tag{6}$$

The points of Fig. 6 are the measured damping constants from the data sets of Fig. 5 for pressures from 0.3 to 1 Torr and series resistances from 2×10^4 to 10^6 Ω. The curves in Fig. 6 show the predicted values of κ for an average of the measured negative discharge differential resistances ($R_D = -4000$ Ω). The dotted lines show the asymptotic limit of κ at low currents, i.e., the first term on the right-hand side of Eq. (6). The vertical lines show the currents for which Eq. (6) predicts $\kappa = 0$ and a transition from damped oscillations to growing or undamped oscillations. The experimental values of κ tend to be either in reasonable agreement with predicted κ values or to be larger than predicted. As discussed in paper I, a slow drift in the quasi-steady-state discharge current I_{SS} during the measurement period can cause the apparent κ values to increase. Except for the two highest current points, the currents at which κ values are obtained from damped oscillations are to the left of the corresponding vertical lines, i.e., the measurements lie within the region of predicted damped oscillations. For example, for $R_S = 10^5$ Ω and $p = 0.5$ Torr the solid squares lie near or above the solid curve, while for $p = 1$ Torr the solid squares lie near or above the dot-dashed curve. The large discrepancy between the κ values measured at the two highest currents for $R_S = 2\times10^4$ Ω is consistent with the failure of the small-signal and the nonlinear models (Sec. III of paper III) to predict the observed transition from undamped oscillations to damped oscillations at currents near 440 μA/cm^2 for 1 Torr shown in Fig. 3. This failure is expected because of the very large space-charge-induced distortion of the electric field at these currents and pressure. Note that the experimental values of κ are rather close to the asymptotic limit of $1/2R_SC$, so that unless the data is considerably more precise than ours it

is difficult to determine R_D from Eqs. (3)–(5).

The equivalent discharge inductance is calculated from the measured angular frequencies ω, circuit capacitance C, and discharge differential resistance R_D using Eqs. (3) and (4). According to Eq. (4), the equivalent inductance L is inversely proportional to the steady-state current I_{SS} so that the quantity LI_{SS} should be independent of current. The experimental values of LI_{SS} shown by the solid points in Fig. 8 are calculated from all of the ω values measured after reliable operation of the experiment was obtained. The close grouping of the points for 0.3 and 0.5 Torr shows that the expected scaling with current is verified. The variation of the LI_{SS} values with breakdown voltage V_B is attributed to the changes in cathode condition. The higher group of LI_{SS} values shown in Fig. 8 for 1 Torr, including that from current growth data discussed in Sec. VI, are all for currents ≥ 1.5 mA (50 μA/cm^2). The lower group of points are for currents ≤ 0.8 mA (16 μA/cm^2). This difference suggests that the small-signal model is beginning to fail at the higher currents at this pressure. Figure 8 shows that the current-normalized inductance decreases with increasing pressure, while Sigmond [15] found this quantity independent of pressure. An inverse dependence of LI_{SS} on pressure has been reported by Weston [24] at high discharge currents where the cathode fall is well developed.

Figures 8 and 9 show the dependence of the current-normalized discharge inductance LI_{SS} and the negative discharge differential resistance $(-R_D)$ on the breakdown discharge voltage V_B for various discharge pressures. The changes in discharge voltage presumably occur because of changes in the cathode condition, e.g., changes in the ion-induced secondary-electron yield. We

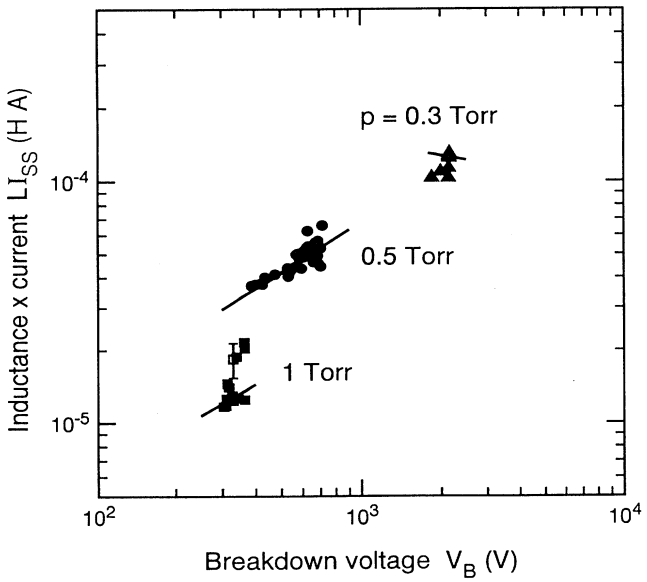

FIG. 8. Normalized discharge inductance vs breakdown voltage for various pressures. The symbols and pressures are ▲, 0.3 Torr; ●, 0.5 Torr; ■, 1 Torr. The open square for 1 Torr is calculated from the fit to experiment in Fig. 10. The solid lines are calculated curves from paper III.

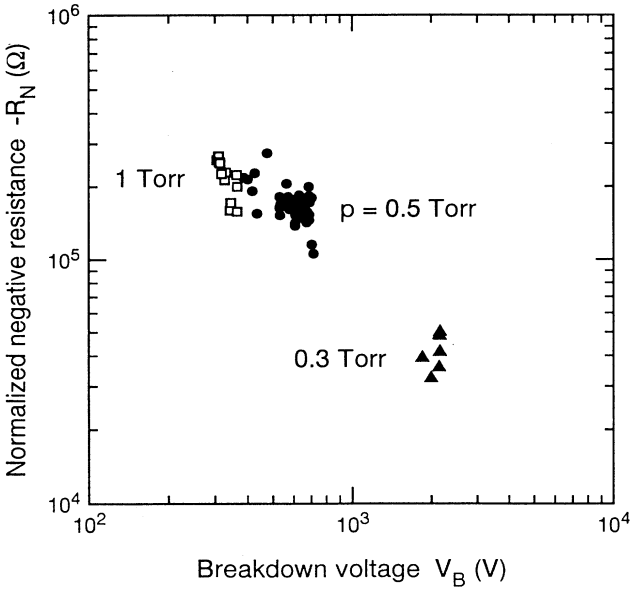

FIG. 9. Normalized negative discharge differential resistance vs breakdown voltage for various pressures. The symbols and pressures are ▲, 0.3 Torr; ●, 0.5 Torr; □ 1 Torr.

were unable to distinguish changes in discharge parameters caused by the buildup of impurities for as long as overnight from changes apparently caused by cathode effects. The particularly large range of discharge voltages observed at 0.5 Torr is the result of the slow variation in the spatial (Townsend) ionization coefficient with E/n [14,20] for $E/n \approx 3$ kTd. For example, a small decrease in the secondary-electron yield caused by a change in cathode condition is compensated by a small increase in ionization coefficient for steady-state operation. For a slowly increasing ionization coefficient with E/n or V, this requires a large increase in V.

The data of Fig. 8 show that for a fixed pressure the normalized inductance LI_{SS} increases with discharge voltage. The discharge differential resistance, on the other hand, tends to decrease with increasing voltage at the higher pressures, but the scatter is large. As the pressure is increased, the average value of the normalized inductances decreases rapidly, while the magnitude of the discharge differential resistance increases. The solid curves of Fig. 8 show the results of the model of paper III after fitting to experiment at one value of the breakdown voltage V_B. These results and the discharge differential resistance will be discussed in paper III.

VI. CURRENT GROWTH

An additional source of information regarding low-current discharges is the growth of current following the application of voltage. Previous measurements for H_2 include the formative time-lag data of Morgan and Llewellyn-Jones and Jones [6] and the times for exponential current growth of Graf and Schmitz [7]. The same basic information can be obtained from the growth of discharge current immediately following the application

of the voltage pulse to the circuit of Fig. 1. In this case the voltage across the discharge initially increases linearly with time, so that the interpretation of the current is more involved than when a step function of voltage is used [6,7]. Thus, in paper III it is shown that the current varies as

$$\ln\left[\frac{I}{I_0}\right]=\frac{1}{T}\frac{\partial g}{\partial V}\int_0^t V(t)dt=\frac{1}{T}\frac{\partial g}{\partial V}at^2\ , \tag{7}$$

where for the short times of interest $V(t)=at$.

Figure 10 shows that Eq. (7) gives a good description of the current growth in H_2 for 1 Torr for a 20:1 ratio of I_0 values, i.e., that the logarithm of the current varies as the square of time. These data are obtained using an improvement in the experiment of Fig. 1 in that a bridge circuit [12] is used to balance out the displacement current flowing through the discharge capacitance. The overall behavior of the current and voltage for the $I_0=2$ $\mu A/cm^2$ case is shown by the inset in Fig. 10. The straight line of Fig. 10 compares Eq. (7) to the data and yields a value of $(1/T)\partial g/\partial V=5.4\times10^4\ s^{-1}V^{-1}$ and, according to Eq. (4), corresponds to $LI_{SS}=1.84\times10^{-5}$ H A. This result is shown by the open square for 1 Torr in Fig. 8. Using the data of the Appendix of paper III to estimate $\partial g/\partial V$, we calculate T to be ≈0.1 μs. This short time is roughly consistent with the free-fall motion of H^+ ions across the 1-cm gap with the applied voltage of ≈450 V, i.e., at $E/n>700$ Td [25].

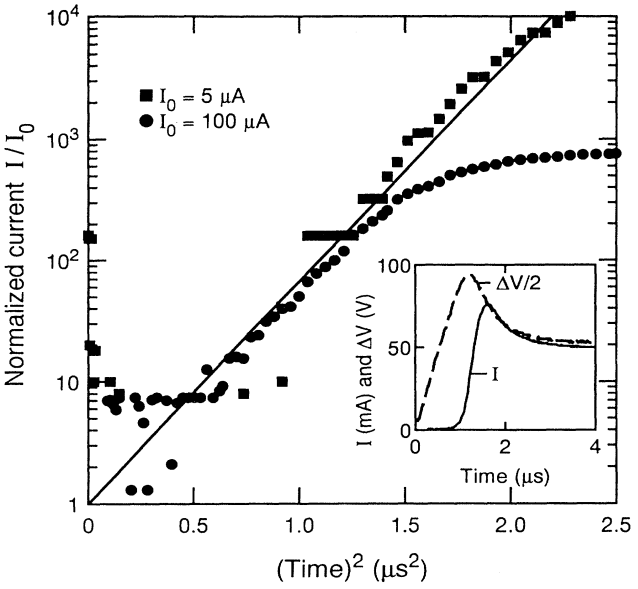

FIG. 10. Discharge current growth in H_2 immediately after application of voltage pulse to circuit. The points are from experiments at 1 Torr with $R_S=20$ kΩ. The squares and circles are for $I_0=0.1$ and 2 $\mu A/cm^2$, respectively. The straight line compares Eq. (7) to the data. The inset is a linear plot of the current and voltage wave forms for $I_0=2$ $\mu A/cm^2$.

VII. DISCUSSION

The experiments with pulsed hydrogen discharges at low pressures and low to moderate currents described in this paper show that (i) these discharges have the voltage-current characteristics of a constant negative differential resistance for wide ranges of current, (ii) voltage pulses produce damped oscillations for discharge currents below those at which oscillation growth is observed, (iii) the frequency of the induced oscillations varies approximately as the square root of the discharge current, (iv) the damping of the oscillations is in approximate agreement with a simple model, and (v) the measured values of the breakdown or low-current discharge voltage, the negative differential resistance of the discharge, and the apparent photoelectric threshold of the cathode are very sensitive to the history of the discharge, especially the cathode.

We have interpreted the measured values of the angular frequencies and damping constants of the transient oscillations in terms of a simple model. The agreement of the measurements with the model for the reasonable parameters indicates that the model is a useful tool in understanding the measurements in terms of gas transport and ionization coefficients and electrode properties, such as ion-induced secondary-electron yields. The pulse technique significantly reduces the ion bombardment of the cathode and so offers the possibility of a nonintrusive diagnostic. We have recently [12] extended the measurements to currents of most practical discharges, e.g., the inset of Fig. 10, and are comparing the results with the available models.

ACKNOWLEDGMENTS

The authors thank A. Gallagher, A. Garscadden, and Z. Lj. Petrović for helpful discussions. They also thank T. J. Brown, T. H. Fung-a-Fat, J. D. Krakover, and J. Csotty for help with the electronics, the computer programming, and modification of the discharge tube. This work was supported in part by the U.S. Air Force Wright Laboratories, the National Institute of Standards and Technology, and the U.S.-Yugoslavia Joint Board, Project No. 924.

*Present address: Institute of Physics, P.O. Box 57, Belgrade, Yugoslavia.
†Permanent address: Central Research Institute of Physics, Budapest, Hungary.
‡Also with Physics Department, University of Colorado, Boulder, CO 80309-0390.

[1] Z. Lj. Petrović and A. V. Phelps, preceding paper, Phys. Rev. E **47**, 2806 (1993); referred to as paper I.
[2] A. V. Phelps, Z. Lj. Petrović, and B. M. Jelenković, following paper, Phys. Rev. E **47**, 2825 (1993); referred to as paper III.
[3] D. Turnquist, R.Caristi, S. Friedman, S. Merz, R. Plante,

and N. Reinhardt, IEEE Trans. Plasma Sci. **PS-8**, 185 (1980).

[4] B. M. Penetrante and E. E. Kunhardt, J. Appl. Phys. **59**, 3383 (1986).

[5] See, for example, K. Frank, in *Physics and Applications of Psuedosparks,* edited by M. A. Gundersen and G. Schaefer (Plenum, New York, 1990), p. 15. See also other papers in this volume.

[6] C. G. Morgan, Phys. Rev. **104**, 566 (1956); F. Llewellyn-Jones and E. Jones, Proc. Phys. Soc. **75**, 762 (1960); E. Jones and F. Llewellyn-Jones, *ibid.* **80**, 450 (1962).

[7] L. Graf and G. Schmitz, Z. Phys. **170**, 418 (1962); L. Graf, in *Proceedings of the Fifth International Conference on Ionization Phenomena in Ionized Gases, Munich, 1961,* edited by H. Meacker (North-Holland, Amsterdam, 1962), p. 1585.

[8] H. Schlumbohm, Z. Naturforsch. **22a**, 347 (1967); **22a**, 1255 (1967).

[9] M. Nahemow and N. Wainfan, J. Appl. Phys. **34**, 2988 (1963).

[10] M. Nahemow, N. Wainfan, and A. L. Ward, Phys. Rev. **137**, A56 (1965).

[11] B. N. Klyarfel'd, L. G. Guseva, and A. S. Pokrovskaya-Soboleva, Zh. Tekh. Fiz. **36**, 704 (1965) [Sov. Phys. Tech. Phys. **11**, 520 (1966)].

[12] B. M. Jelenković and A. V. Phelps (unpublished); in *Proceedings of the Tenth International Conference on Gas Discharges and Their Applications, Swansea, Wales, 1992,* edited by W. T. Williams (University of Swansea, Swansea, Wales, 1992), p. 513.

[13] See for example, M. M. Kekez, M. R. Barrault, and J. D. Craggs, J. Phys. D **5**, 253 (1972).

[14] M. A. Folkhard and S. C. Haydon, Aust. J. Phys. **24**, 517 (1971); **24**, 527 (1971); Z. Stokic, M. M. F. R. Fraga, J. Bozin, V. Stojanović, Z. Lj. Petrović, and B. M. Jelenković, Phys. Rev. A **45**, 7463 (1992).

[15] R. S. Sigmond, in *Proceedings of the Fourth International Conference on Ionization Phenomena in Gases, Uppsala, 1959,* edited by N. R. Nilsson (North-Holland, Amsterdam, 1960), p. 189; in *Proceedings of the Fifth International Conference on Ionization Phenomena in Gases, Munich, 1961* (Ref. [7]), p. 1359; in *Proceedings of the Ninth International Conference on Ionization Phenomena in Gases, Bucharest, 1969,* edited by G. Musa, I. Ghica, A. Popescu, and L. Nästase (Institute of Physics, Academy of Socialist Republic of Roumania, Bucharest, 1969), p. 129.

[16] See papers I and III for reviews of earlier experimental and theoretical work on these oscillations.

[17] Z. Lj. Petrović, B. M. Jelenković, and A. V. Phelps, Phys. Rev. Lett. **68**, 325 (1992).

[18] D. E. Davies and R. K. Fitch, J. Appl. Phys. **10**, 502 (1959); G. S. Selwyn, B. D. Ai, and J. Singh, Appl. Phys. Lett. **52**, 1953 (1988).

[19] We have avoided the terminology of photoelectric work function because of practical difficulties in determining the work function from measurements of photocurrent versus photon energy. See, for example, G. L. Weissler, Handb. Phys. **21**, 345 (1956); A. L. Hughes and L. A. DuBridge, *Photoelectric Phenomena* (McGraw-Hill, New York, 1932), Chap. 6.

[20] M. J. Druyvesteyn and F. M. Penning, Rev. Mod. Phys. **12**, 87 (1940).

[21] G. Francis, Handb. Phys. **22**, 53 (1956).

[22] H. Niesters, in *Proceedings of the Fourth International Conference on Ionization Phenomena in Gases, Uppsala, 1959* (Ref. [15]), p. 175.

[23] D. J. DeBittetto, L. H. Fisher, and A. L. Ward, Phys. Rev. **118**, 920 (1960); A. L. Ward and E. Jones, *ibid.* **122**, 376 (1961). Sigmond [15] suggests that some published data are seriously in error because of undetected oscillations, e.g., C. G. Morgan and E. Jones, quoted in F. Llewellyn-Jones, *Ionization and Breakdown in Gases* (Methuen, London, 1957), p. 60.

[24] G. F. Weston, in *Proceedings of the Fifth International Conference on Ionization Phenomena in Ionized Gases, Munich, 1961* (Ref. [15]), p. 528.

[25] A. V. Phelps, J. Phys. Chem. Ref. Data **19**, 653 (1990).